ADVANCED FUNCTIONAL MATERIALS
www.afm-journal.de

Check for updates

A Highly-Adhesive and Self-Healing Elastomer for Bio-Interfacial Electrode

Zhicheng Xu, Litong Chen, Liangliang Lu, Ruichun Du, Wencan Ma, Yifeng Cai, Xiaoming An, Haomin Wu, Qiong Luo, Qiang Xu, Qiuhong Zhang, and Xudong Jia**

Stretchable electrodes are playing important roles in the measurement of bio-electrical signals especially in wearable electronic devices. These electrodes usually adopt commercial elastomers such as polydimethylsiloxane or polystyrene-ethylene-butylene-styrene as substrates, which result in poor stability and reliability due to weak interfacial adhesion between electrodes and human skin. Here, dopamine is introduced into the hydrogen bonding based elastomer as pendent groups. The elastomer shows both mechanical strength and adhesion strength at the same time. It exhibits high stress at break (1.9 MPa) and high fracture strain (5100%). Significantly, it exhibits a high adhesive strength (≈62 kPa) and underwater adhesive strength (≈16 kPa) with epithelial tissue. Thus, a stretchable bio-interfacial electrode is fabricated by spray-coating silver nanowires on the elastic substrate, which is stretchable, self-healable, and highly adhesive and suitable for electromyogram measurement.

1. Introduction

The nerve activity and muscle movement of organisms are accompanied by very weak electrical current[1] and electrical potential changes,[2] which are known as bioelectric current.[3,4] The measurement of bioelectric current usually provides important information of organisms[5] which will help doctors to diagnose the condition of a patient. Interfacial electrodes which are key devices[6,7] to collect the electrical signals like electrocardiogram or electromyogram (EMG). Commercial electrodes like rigid electrodes[8] are used to measure the bioelectricity by penetrating into the tissue detrimentally. Compared to the rigid interfacial electrodes, soft electrodes[9] have a great advantage that they can be widely used in wearable devices, because of their soft and stretchable properties which enable application on different parts of the human body and greatly reduce pain in clinical treatment.

In recent years, several substrates have been used to fascinate in the study of soft interfacial electrodes, such as polydimethylsiloxane (PDMS),[10] polyimide (PI),[11] polyethylene terephthalate (PET),[12] et cetera. Compared to PI and PET, PDMS and SEBS based substrates can easily form a conformal interface with the human skin. Beak et al.[13] deposited a layer of metal on PDMS substrate, and fabricated the wearable electrode on the forearm by etching the electrode patterns chemically. Jung et al.[14] developed PDMS-based dry type surface electromyography (SEMG) electrode for myoelectric prosthetic hands. The dry type flexible SEMG electrode showed higher peak values than commercially wet type Ag/AgCl electrodes. Yan et al.[15] made a stretchable electrode by evaporating micro-cracked gold thin film on a 2-ureido-4-pyrimidinone based polymer, and used it in the SEMG. These electrodes showed very good conductivity and could test the sensitive signals well. However, these electrodes usually showed poor performance for long-time monitoring, especially when the body moved, due to poor interfacial adhesion between tissue and electrode.[15] Simultaneously, reducing contact impedance is an important factor to acquire reliable signals. Therefore, to promise stable and reliable measurements, stretchable interfacial electrode should also be endowed with high adhesion property.

Marine mussels[16] have mastered the ability of anchoring to various surfaces by use of adhesive proteins.[17–19] These mussel foot proteins[20–22] can solidify rapidly to form adhesive plaques with high interfacial binding durability and toughness. The 3,4-dihydroxyphenylalanine (Dopa) plays a key role in adhesion mechanism[23,24] which enables it to bond tightly to diverse surfaces through the formation of reversible noncovalent and irreversible covalent interactions, including H-bonds,[25] π–π electron interaction,[26] cation-π interaction,[27] co-ordination,[28–30] and a series of covalent crosslink via Dopa oxidation products.[31–35] The dihydroxy[25] of catechol can form

Z. Xu, L. Chen, R. Du, W. Ma, Y. Cai, X. An, H. Wu, Prof. Q. Zhang, Prof. X. Jia
Key Laboratory of High Performance Polymer Material and Technology of MOE
Department of Polymer Science and Engineering
School of Chemistry and Chemical Engineering
Nanjing University
Nanjing 210023, P. R. China
E-mail: chemzqh@nju.edu.cn; jiaxd@nju.edu.cn
L. Lu, Dr. Q. Luo, Prof. Q. Xu
State Key Laboratory of Pharmaceutical Biotechnology
School of Life Sciences
Nanjing University
Nanjing 210023, P. R. China
Prof. X. Jia
State Key Laboratory of Coordination Chemistry
Nanjing University
Nanjing 210023, P. R. China
The ORCID identification number(s) for the author(s) of this article can be found under https://doi.org/10.1002/adfm.202006432.

DOI: 10.1002/adfm.202006432

© 2020 Wiley-VCH GmbH

strong bidentate hydrogen bonds with proteins, promoting its rapid and stable adhesion to the tissues. And the bond lifetime and binding energy of bidentate hydrogen bond are much longer and higher than those of mono-dentate hydrogen bond according to the calculation and certification based on Bell theory and surface force apparatus.[36] The benzene ring of catechol is capable of interacting with aromatic amino acids through π–π electron interaction[26] or positively charged amino acids through cation–π interaction.[27] More importantly, once oxidized in air to semiquinone or quinone, it can react with the amine or thiol groups widely spread on the tissue surface to form stable covalent linkage.[31–35] Catechol moiety had been incorporated into a lot of hydrogel systems,[37–40] however, the elasticity and strength usually showed modest performances.

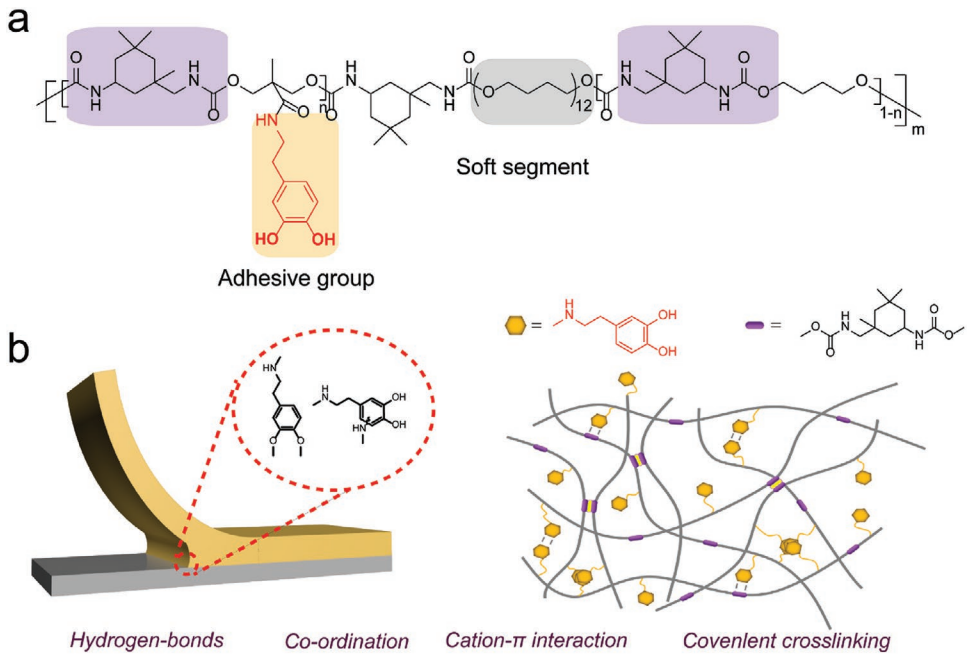
Inspired by mussels, we incorporated the biocompatible[41–43] dopamine (DA) into a urethane based polymer and obtained a stretchable and highly adhesive elastomer. The elastomer exhibits a high mechanical strength of 1.9 MPa, and at the same time, it shows good adhesion to various materials especially high adhesive strength (≈62 kPa) with porcine skin. Simultaneously, the high adhesive strength could still maintain ≈54 kPa even after being soaked in water for 24 h. Furthermore, we fabricated an interfacial electrode by spray-coating AgNWs[44] on our elastomer and used it for in the vitro monitoring of EMG.

2. Molecular Design

To meet the stretchable and adhesive requirements of the interfacial electrode, the material should be endowed with both adhesive ability and stretchability. Initially, we synthesized DMPA-DA which could react with diisocyanates, thereby endowing the material with adhesive ability (**Scheme 1**) (synthetic route and ^{1}H NMR as referred to in Figure S1–S5, Supporting Information). The urethane linked polymer can form microphase-separated structure,[45] which endows the material with elastic property. Therefore, the elastomers with high adhesion can be obtained by tuning the proportion of hard segments, soft segments, and the chain extenders of the designed materials. Here, we chose isophorone diisocyanate (IPDI) and polytetramethylene glycol (PTMG) as the hard and soft segment of the polymer respectively (Scheme 1). The modulus of the designed polymer could be tuned to be compatible with human skin, which would be more applicable in bio-interfacial electrode.[15] In order to optimize elastomers' properties, we had synthesized a series of elastomers by controlling the molar ratio of DMPA-DA and 1,4-butanediol. The increasing molar ratio of DMPA-DA, dopamine pendent elastomers (DAEs) were termed as DAE-0, DAE-1, DAE-2, DAE-3, DAE-4 (detailed information is shown in Table S1, Supporting Information). ^{1}H NMR (Figure S6, Supporting Information) indicated that DMPA-DA successfully participated in polymerization. Moreover, the absence of the typical NCO peak (2260 cm^{-1}) in FT-IR (Figure S7, Supporting Information) suggested the complete reaction of the pre-polymers. Besides, the stretching vibration band of C=O in DMPA-DA at 1650 cm^{-1} indicated that DMPA-DA was successively incorporated into the polymer (Figure S8, Supporting Information).

3. Rheological and Mechanical Properties

We performed small angle X-ray scattering (SAXS) for DAE-0 and DAE-3. For DAE-0, it showed a very weak halo which suggested a nearly homogenous structure of the system. When DMPA-DA was introduced into the polymer, it displayed a visible broad scattering peak at around 0.1 Å, indicating that the introduction of DMPA-DA increased the degree of micro-phase



Scheme 1. a) Molecular structure of dopamine (DA)-pendent urethane based elastomer. b) A schematic depiction of DAE that contained adhesion moiety and hydrogen bond moiety.

© 2020 Wiley-VCH GmbH

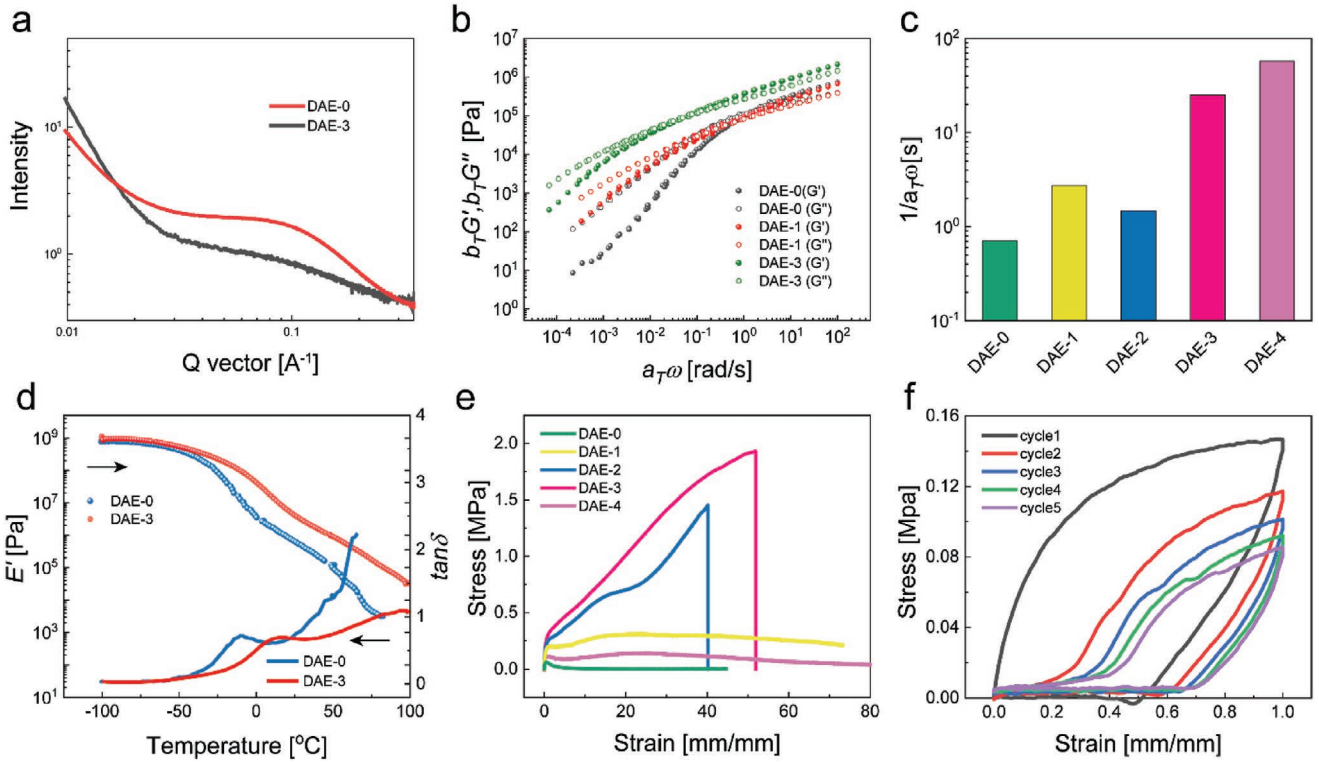


Figure 1. a) SAXS of DAE-0 and DAE-3. b) Master curves of the DAEs shifted according to time-temperature superposition. Frequency sweep of the DAEs, was performed from 100 to 20 °C with an interval of 20 °C over a span of three decades of frequency between 0.628 and 628 rad s^{-1} (reference temperature 20 °C, 1% strain). c) The relaxation time of DAEs. d) DMA for DAEs with different DA ratios. e) Stress-strain curves of the DAEs elastomer. f) Cyclic loading and recovery of DAE-3. The samples were conducted cyclic loading for 5 times (100% strain) at a tensile rate of 5 mm min^{-1}.

separation. The average distance between the ordered domains was about 6.9 nm (**Figure 1**a). The enhancement of the microphase separated structure would improve the mechanical properties of elastomers (Figure 1b–d).

Frequency dependent complex moduli of samples at different temperatures were scaled onto master curves by time temperature superposition (TTS). All DAEs showed viscoelastic properties with storage modulus (G') and loss modulus (G'') crossing at ω_c. At lower frequency ($\omega < \omega_c$), G'' was higher than G' which indicated DAEs possessed viscous property. When $\omega > \omega_c$, it showed solid property (Figure 1b). Particularly, when increasing the molar ratio of DA from 0% to 15%, both of G' and G'' of DAEs increased gradually (Figure S9, S10, Supporting Information, and Figure 1b). Moreover, with the increasing content of DMPA-DA, the terminal relaxation time of most of the DAEs (τ_c) increased gradually, which showed the increasing trend of crosslinking density of DAEs with the DMPA-DA increased (Figure 1c). Dynamic mechanical analysis (DMA) exhibited that DAEs have higher storage modulus and glass transition temperature (T_g) than DAE-0 (Figure S11 and S12, Supporting Information). It was attributed to the introduction of DMPA-DA, which increased the crosslinking density of the elastomers and hindered the mobility of the polymer chain.

The stretchability of the elastomer played an imperative role in the soft electrodes. In order to optimize the elastomers' properties, a tensile test was conducted to characterize the mechanical properties of DAEs (Figure 1e). We found that the mechanical properties of DAEs showed a big difference when varying the molar ratios of DMPA-DA. DAE-0 had a relatively weak strength (<0.05 MPa) and behaved like a fluid liquid when stretched to a higher strain. Upon increasing DMPA-DA ratio, the mechanical strengths of DAE-2 and DAE-3 were dramatically improved compared to that of DAE-0. As observed from Figure 1e, DAE-3 showed the highest mechanical property that it could be stretched up to 5000% with the fracture strength of 1.9 MPa. The enhancement in mechanical strength could be ascribed to the increased crosslinking density originating from the interactions between dopamine groups. However, when further increasing the molar ratio of DMPA-DA, such as DAE-4, it showed a weakened mechanical property (Figure 1e). We ascribed the reason to it that higher content of DMPA-DA would cause the effective reaction of the chain extender to decrease, therefore losing the packing density of the molecular chain. Moreover, cyclic tensile tests were performed (Figure 1f and Figure S13, Supporting Information), which was stretched to 2 times its original length for 5 cycles. The hysteresis occurred in each cycle and the Young's modulus of the polymer decreased gradually in each cycle, indicating the dissipation of the dissociation of the hydrogen bond during stretching. The DAEs had lower energy dissipations than DAE-0 at 100% strain during the first cycle (Figure S14, Supporting Information), indicating better elasticity when DMPA-DA was introduced.

© 2020 Wiley-VCH GmbH

4. Adhesion Properties

We characterized the adhesive strength of the materials with tissue (**Figure 2**). Porcine skin was used as the test substrate due to similar biological properties with the human dermis. We observed that the adhesive strength of DAEs increased continuously with the increasing of DMPA-DA ratio, and DAE-4 exhibited the highest adhesive strength of 71 kPa (Figure 2a,b and Figure S15, Supporting Information). It had been reported that the outstanding adhesion performance of dopamine-functionalized polymers was due to the formation of covalent bonds[46,47] as well as the physical interactions with the materials.[16,48,49] To further prove that the strong adhesion was from the presence of catechol groups, we synthesized a control sample (Pro-DAE) which contained chain extender (Pro-DMPA-DA) with protected phenolic hydroxyl groups. The synthetic route and ^{1}H NMR of Pro-DMPA-DA are shown in Figure S16–S18, Supporting Information. We observed that the adhesive strength of Pro-DAE was lower than that of DAE-3, though it contained the same molar ratio of the substituents (Figure S19, Supporting Information). It proved that the existence of phenol groups[16,46,47] on dopamine could contribute to enhance the adhesive strength of DAEs. In addition, the adhesive strength of Pro-DAE was higher than that of DAE-0, which meant that the amide group[50] in Pro-DMPA-DA could also increase the adhesive strength by forming H-bonds. Furthermore, the adhesion process of DAE-3 was carried out under different atmospheres (nitrogen, air, and oxygen) for the same amount of time.

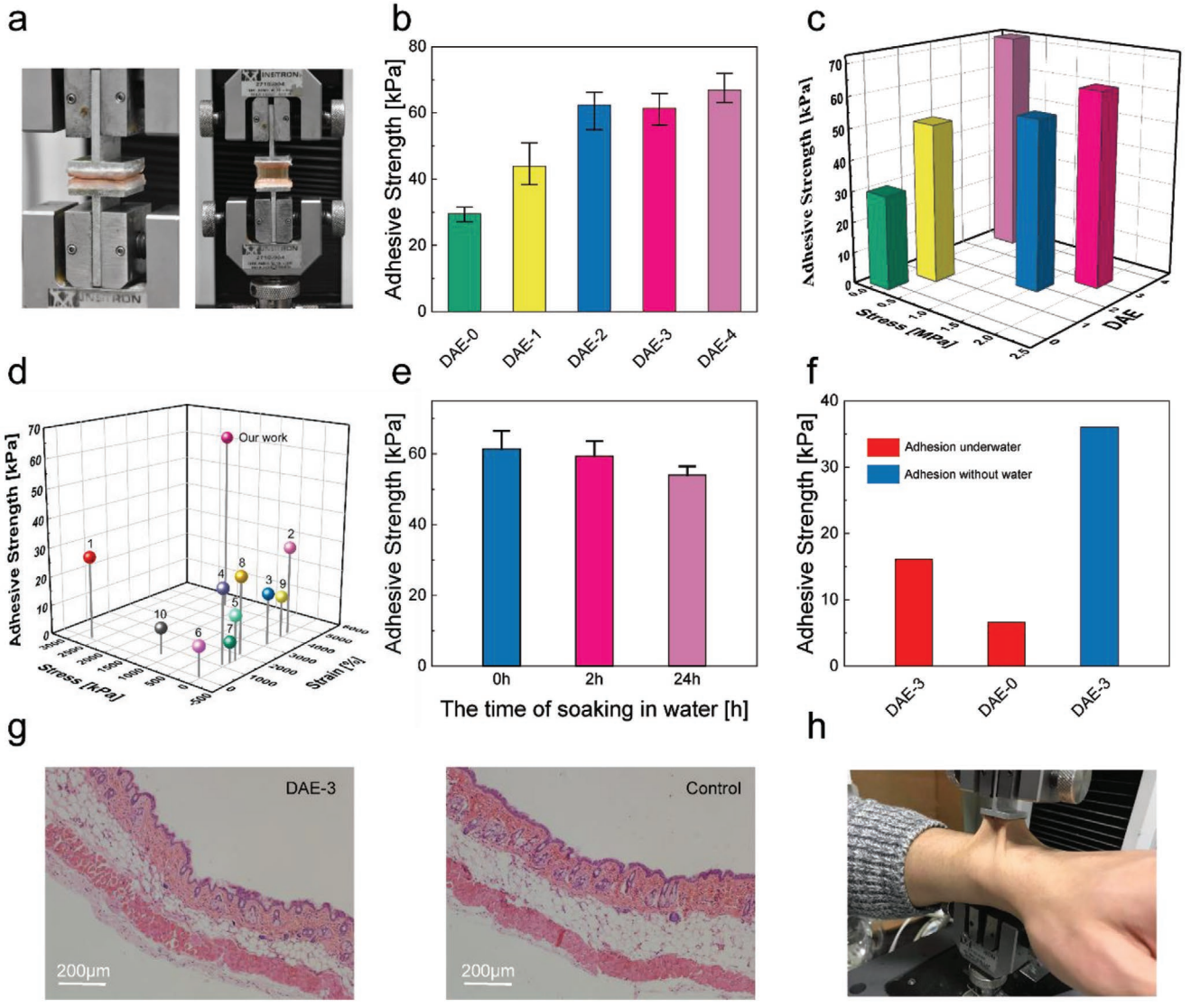


Figure 2. Adhesion properties of the DAEs. a) Standard test fixtures for strength properties of tissue adhesives in tension (load the specimen to failure at a constant cross-head speed of 5 mm min^{-1}). b) Adhesive strength of the DAEs. c) Mechanical properties and adhesive strength of the DAEs. d) Comparison of the strain, stress, and adhesive strength of the DAE-3 with other adhesive polymers reported recently: 1 (ref. [19]), 2 (ref. [35]), 3(ref. [48]), 4 (ref. [49]), 5 (ref. [50]), 6 (ref. [51]), 7 (ref. [52]), 8 (ref. [53]), 9 (ref. [54]), 10 (ref. [55]). e) Adhesive strength of DAE-3 after soaking in water with different time. f) The adhesive strength of under-water adhesion. g) Histological microscopy images of skin adhered by DAE-3 (left) and control sample (right) (H&E staining). h) The photo of strong adhesion between the DAE-3 and human skin.

© 2020 Wiley-VCH GmbH

We could observe that the adhesive strength of DAE-3 (N_2) was lower than that of DAE-3 (O_2), which meant that the covalent crosslinking[48,49] between oxidized dopamine and amine group on the tissue would also contribute to the increase in adhesion strength (Figure S20, Supporting Information).

The mechanical strength and adhesion strength are important factors to an elastic adhesive. To optimize the properties for tissue adhesive, we plotted mechanical strength and adhesive strength as the dopamine groups' content changed (Figure 2c). Considering the electrode in practical application, we chose DAE-3 which possessed higher stress and adhesive strength at the same time as our electrode material in the following research. Simultaneously, we compared the mechanical properties of recently reported stretchable and adhesive materials[19,35,50–57] with our material, and found it could both exhibit high stretchability and realize high adhesion with porcine skin at the same time (Figure 2d).

As we know, for a commercial electrode, the adhesion strength of the adhesive usually decreases rapidly when people sweat due to the penetration of water into the skin-electrode interfacial. The strategy of introducing hydrophobic segments into the adhesive showed a great advantage in achieving a high strength under water.[58] The hydrophobicity induced by hydrophobic segments could dispel the hydrated water on the interface, leading to an enhancement of the interaction of adhesive groups with the adherent and thus stabilizing underwater adhesion.[59,60] Therefore, considering the hydrophobic property of the PTMG in DAEs, we further evaluated the wet adhesion property of DAE-3. As expected, DAE-3 still maintained strong adhesion even after being soaked in water for 24 h (Figure 2e), which showed the potential application for wet adhesion. Subsequently, in order to further test and verify the under-water adhesive ability of DAE-3, we performed a test (Figure S21, Supporting Information) according to the American Society of Testing Materials ASTM F2558-05(2015). Porcine skin was stuck to the test fixture and the container by gel–type cyanoacrylate adhesives, followed by adding water into the container until the adhesive layer and fixture were covered. The DAE-3 was then used as an adhesive layer and stuck onto the porcine skin underwater with an applied force of ≈2 N for 2 h. It showed that DAE-3 could still maintain good adhesive strength (19 kPa) under water (Figure 2f). The result indicated that the material may possess adhesiveness under a wet environment. In our work, the good adhesion under water was ascribed to the hydrophobic property of a soft segment which prevented water permeation. To visualize the water barrier mechanism, a DAE-3/PAA gel/PDMS and commercial electrode/PAA gel/PDMS sandwich structure was prepared and immersed in dyed solution (AO7, 0.2% v/v). After 30 min, we observed the dye diffused into the interface between the commercial gel electrode and PDMS, while the dye diffusion was not observed between DAE-3 and PDMS (Figure S22, Supporting Information).

As bio-interfacial electrodes, biocompatibility is also an essential factor for actual application, a murine model was used to evaluate the in vitro biocompatibility of DAEs. DAEs were attached to the depilated dorsal skin of mice and secured with a medical bandage for 2 days (Figure S23, Supporting Information). There was no obvious irritative reaction (such as erythema, swelling, etc.) on the skin that attached with DAEs. The skin samples were further analyzed by hematoxylin and eosin (H&E) staining. Histological analysis (Figure 2g and Figure S23, Supporting Information) showed that DAEs did not induce structural changes in the skin. There was no significant difference in the thickness of the dermis and the epidermis layers in the control sample and DAEs groups. In addition, the adnexal structures in DAEs-attached skin were similar to those of the control groups' skin. The bio-compatibility of DAEs was further confirmed by cytocompatibility experiments. (Figure S24 and S25, Supporting Information)

We have confirmed that DAE-3 had a good biocompatibility, and strong adhesive strength with human skin (Figure 2h and Video S1, Supporting Information). Moreover, the DAE-3 elastomer also exhibited good adhesion with metal, glass, and plastic (Figure S26, Supporting Information). The strong adhesion was attributed to the formation of reversible non-covalent[25,26] or irreversible covalent interaction[61,62] through the abundant catechol groups.[37]

5. Stretchable, Self-Healing, and Highly-Adhesive Bio-Interfacial Electrodes

To make a stretchable and highly adhesive bio-interfacial electrode, we spray-coated silver nanowires (AgNWs) as a conductive layer on top of the elastomer. In order to optimize the best performance of the electrode, we conducted three different concentrations of silver nanowire dispersions to fabricate the stretchable electrodes. As shown in **Figure 3**a, the electrode coated with 0.5 wt% nanowire dispersion (termed as DAE-Ag-0.5 wt%) could keep electrical conductivity even when stretched over 105%, while DAE-Ag-1.5 wt% electrode could only maintain its conductivity under 60% strain. Therefore, we chose the DAE-Ag-0.5 wt% electrode as the reference sample for further demonstrations. We observed that the random distribution of AgNWs on DAE-Ag-0.5 wt% could form a continuous network, which could be maintained even under a strain of 100%. (Figure 3b). Simultaneously, we also evaluated the bio-compatibility of DAE-Ag electrodes. The morphological appearance of the skin attached by the DAE-Ag electrodes was unchanged and showed the presence of a complete epidermis and intact hair follicles (Figure S27, Supporting Information). Moreover, we found that DAE-3 exhibited a stronger adhesion with AgNWs than other elastomers such as PDMS due to the strong metal-ligand coordination[63–66] between dopamine and silver nanowires (Figure S28, Supporting Information).

When the elastomer is applied as an electrode, inevitable damage will happen in practical use. Therefore, a good self-healing property can prolong the service life of the electrode. Interestingly, we found that our elastomer showed a good self-healing ability. We scratched a cross section on the DAE-3 film, and the scratches almost disappeared after healing at room temperature (25 °C) for 12 h (Figure 3c). In order to show it more intuitively, we cut the original and stained it with Sudan III samples. Then, the samples were joined together for healing at room temperature for 24 h, which could still remain in excellent stretchability (Figure 3d). Furthermore, we cut the samples into two pieces and joined them together for healing with different amounts of time. As shown in Figure 3e, the self-healing

© 2020 Wiley-VCH GmbH

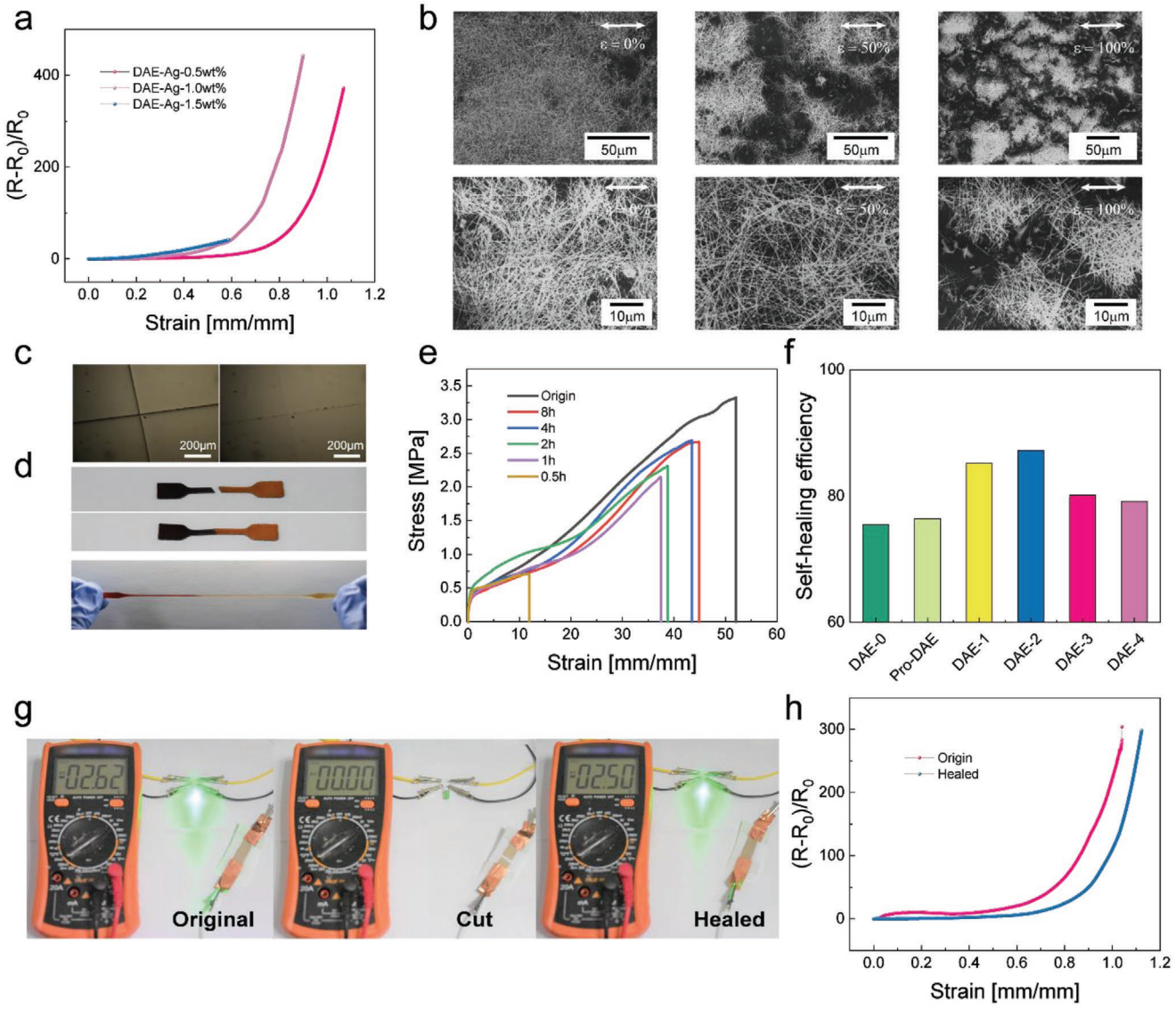


Figure 3. Stretchable, self-healing, and highly-adhesive bio-interfacial electrode. a) The tensile conductivity curves by spray-coating with different concentration of AgNWs. b) SEM images of an AgNWs based electrode during stretching to different strain. c) Optical image of DAE-3 before and after healing at 25 °C for 12 h. Cut depth: 50–60% of its thickness 0.6 mm. d) The sample was healed at room temperature for 12 h after cut into separate pieces and joined together. e) Stress-strain curves of the original and the self-healed DAE-3 specimens after different healing times from 0.5 to 8 h at room temperature. Deformation rate: 20 mm min^{-1}. f) The self-healing efficiency of DAEs after healing for 8 h at room temperature. g) Demonstration of the healing process for a circuit with stretchable electrode based on **DAE-3**. The electrode was cut into completely separate pieces, then they were aligned and the circuit can recover to work immediately. h) The relative resistance changes of the original electrode and self-healed electrode.

efficiency of DAE-3 reached 86% after healing 8 h under 25 °C, if strain was taken into account.

We ascribe the self-healing ability to three aspects. First, polymer chain diffusion and chain mobility play an important role in self-healing ability. From the rheological measurements (Figure 1c), we estimate the timescale (terminal relaxation time) of DAE-3 was about 25 s, which indicated fast polymer chain mobility. Second, dynamic hydrogen bonds also contribute to the self-healing ability of the system. The urethane linkages which were generated from the reaction of IPDI and PTMG, have a much higher content of hydrogen bonding between the N–H and C=O groups, making a great contribution to self-healing. Finally, the introduction of dopamine plays an important effect on the high self-healing efficiency. We performed the self-healing experiments on samples with different contents of dopamine groups (Figure S29–S32, Supporting Information), and the self-healing efficiency for 8 h at 25 °C were summarized in Figure 3e. It was observed that self-healing efficiency of DAE-0 reached 75.5% after healing for 8 h, and other DAE samples with different contents of dopamine groups had higher healing efficiency. We thought the phenol of dopamine in elastomer offered more H-bonds[48,67] and the π-π stacking.[26,68] Then we observed that Pro-DAE had a lower self-healing efficiency (76.4%) than other

© 2020 Wiley-VCH GmbH

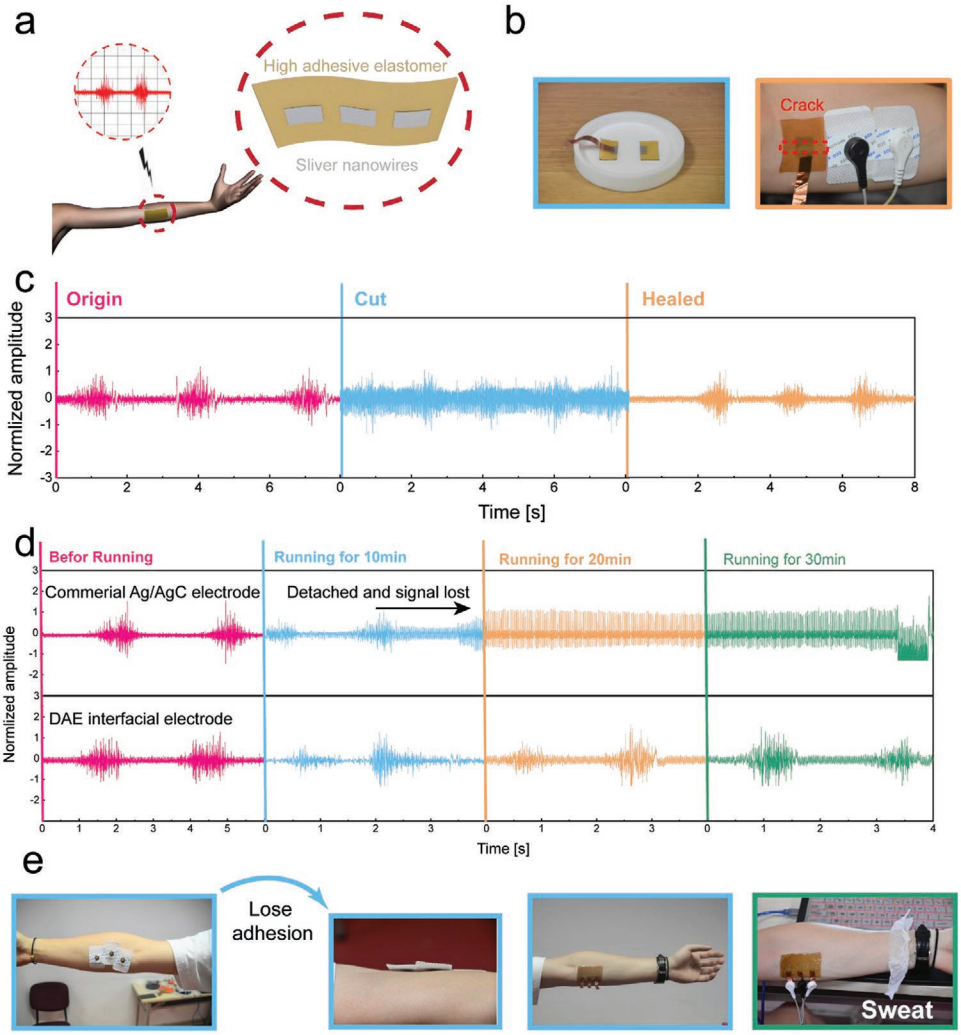


Figure 4. Stretchable, highly-adhesive, bio-interfacial electrode on-skin EMG monitoring. a) A schematic depiction of the on-skin EMG detected and measured energy spectrum analysis of the EMG signal. b) Photos of DAE electrode cut and after healing. c) Ambulatory EMG monitoring when DAE electrode was cut off and after healing. d) Ambulatory EMG monitoring after different sport times obtained by DAE and commercial gel electrodes under sweaty conditions. e) Photos of the adhesion of DAE electrode and commercial gel electrode after running for different times.

dopamine-contained-DAEs, which proved that the existence of free phenol groups in dopamine could facilitate the self-healing efficiency through coupling between dopamine groups. It indicated that the addition of dopamine in the material promoted the self-healing of DAEs.

To evaluate the self-healing ability of DAE-Ag electrode, we used our DAE-Ag-0.5 wt% electrode and LED to build a circuit, and a 3.0 V voltage was applied on the circuit. As expected, the LED turned off when the electrode was cut. But, after splicing the two pieces of electrodes together, the LED was observed to turn on again (Figure 3g). Furthermore, we also measured the resistance change during stretching before and after healing (Figure 3h). It showed that the stretchable conductor could also be extended over 100% strain after healing.

Next, we demonstrated an EMG based on our elastic and adhesive electrode (**Figure 4**a). The obtained EMG signals are comparable to commercial Ag/AgCl gel electrodes (Figure S33, Supporting Information). Therefore, we successfully demonstrated the potential application of our stretchable and adhesion material for in vitro.

We have known that the stretchable conductor could be healed at room temperature (Figure 3e). To demonstrate the self-healing ability of EMG electrode, here, we cut the electrode (Figure 4b) and the EMG signal immediately became weak and showed low signal/noise ratio due to the increase of resistance (Figure 4c). After healing for 4 h, the signal/noise ratio increased to the original level (Figure 4c and Video S2, Supporting Information). The result showed that our electrode had an ability to respond well to breakage during application, and could keep working smoothly. In addition, we observed the electrode could be peeled off without leaving any residue after EMG monitoring (Figure S34, Supporting Information).

To demonstrate the good adhesion property, the EMG signals of DAE-3 electrode and commercial gel electrode were contrasted during sweating after running for different amounts of time (Figure 4d). Compared with other electrodes,

© 2020 Wiley-VCH GmbH

our electrodes could directly to stick the skin without using other adhesives. We observed that the commercial gel electrode was detached (Figure 4e and Video S3, Supporting Information) and the signal lost after running for 10 min, while the DAE-3 electrode could maintain EMG signal well even running for 30 min under sweaty conditions (Figure 4d,e and Video S4, Supporting Information). The result showed that the DAE-3 electrode had the ability of working under sweaty conditions.

6. Conclusion

In summary, we have designed and synthesized a highly adhesive elastomer that contains dopamine as a pendant group and for hydrogen bonding. The microphase separation elastomer can reach a high mechanical strength and strain by tuning the amount of dopamine. The adhesive strength of the material in the porcine skin increased as the dopamine increased, which can reach 62 kPa in dry state and keep adhesion at wet condition. Due to the dynamic H-bonding and DA groups, we also found the material showed good self-healing ability (86% at 8 h at 25 °C).

Based on the highly adhesive and self-healable elastomer, we fabricated stretchable and high-adhesion interfacial electrodes by spray coating different concentrations of AgNWs on the substrate, and selected the concentration of 0.5 wt% which still maintains conductivity under a strain of 105%. The DAE-Ag-0.5 wt% electrode showed a good self-healing property and could monitor an EMG signal at the original level. Simultaneously, the DAE-3 electrode also showed a good adhesion property with sweat after running for 30 min. The bio-interfacial electrode exhibited stretchable, highly-adhesive, biocompatible, and self-healable properties which may be an ideal alternative for wearable electronics.

Supporting Information

Supporting Information is available from the Wiley Online Library or from the author.

Acknowledgements

The authors thank the National Natural Science Foundation of China (Grants 21875102 and 22075130). The work was also supported by the Fundamental Research Funds for the Central Universities. They also thank Jingyu Yin for the discussions in bio-experiments. Animal welfare and experimental procedures were strictly in accordance with the Guidelines for the Care and Use of Laboratory Animals (National Institutes of Health) and the related ethical regulations of Nanjing University. The medical ethical committee of Nanjing University approved all described studies (IACUC 2007002). The EMG tests were approved by Ethics Committee of Nanjing Drum Tower Hospital affiliated Nanjing University Medical School (IRB 2020-189-01).

Conflict of Interest

The authors declare no conflict of interest.

Keywords

adhesion, dopamine, self-healing, stretchable electrode

Received: July 30, 2020
Revised: September 13, 2020
Published online:

[1] M. D. Ferro, N. A. Melosh, *Adv. Funct. Mater.* **2018**, *28*, 1704335.
[2] G. Buzsaki, C. A. Anastassiou, C. Koch, *Nat. Rev. Neurosci.* **2012**, *13*, 407.
[3] H. Yuk, B. Lu, X. Zhao, *Chem. Soc. Rev.* **2019**, *48*, 1642.
[4] B. Reid, R. Nuccitelli, M. Zhao, *Nat. Protoc.* **2007**, *2*, 661.
[5] Y. M. Chi, T. P. Jung, G. Cauwenberghs, *IEEE. Rev. Biomed. Eng.* **2010**, *3*, 106.
[6] N. Joye, A. Schmid, Y. Leblebici, *Neurocomputing* **2009**, *73*, 250.
[7] A. D. Gilmour, J. Goding, L. A. Poole-Warren, C. E. Thomson, R. A. Green, in *Int. IEEE/EMBS Conf. Neural Eng.*, IEEE, Montpellier, France **2015**, 450.
[8] R. A. Normann, E. Fernandez, *J. Neural Eng.* **2016**, *13*, 061003.
[9] S. Park, M. Vosguerichian, Z. Bao, *Nanoscale* **2013**, *5*, 1727.
[10] C.-Y. Chen, C.-L. Chang, T.-F. Chien, C.-H. Luo, *Sens. Actuators, A* **2013**, *203*, 20.
[11] S. Ichimori, K. Nishida, S. Shimoda, T. Sekigami, Y. Matsuo, K. Ichinose, M. Shichiri, M. Sakakida, E. Araki, *J. Artif. Organs* **2006**, *9*, 105.
[12] S. Yamamoto, M. Honda, T. Oohashi, K. Shimizu, M. Senda, *IEEE Trans. Nucl. Sci.* **2011**, *58*, 668.
[13] J.-Y. Baek, J.-H. An, J.-M. Choi, K.-S. Park, S.-H. Lee, *Sens. Actuators, A* **2008**, *143*, 423.
[14] J. M. Jung, D. Y. Cha, D. S. Kim, H. J. Yang, K. S. Choi, J. M. Choi, S. P. Chang, *Appl. Phys. A: Mater. Sci. Process.* **2014**, *116*, 1395.
[15] X. Yan, Z. Liu, Q. Zhang, J. Lopez, H. Wang, H. C. Wu, S. Niu, H. Yan, S. Wang, T. Lei, J. Li, D. Qi, P. Huang, J. Huang, Y. Zhang, Y. Wang, G. Li, J. B. Tok, X. Chen, Z. Bao, *J. Am. Chem. Soc.* **2018**, *140*, 5280.
[16] P. Kord Forooshani, B. P. Lee, *J. Polym. Sci., Part A: Polym. Chem.* **2017**, *55*, 9.
[17] J. H. Waite, *Int. J. Adhes. Adhes.* **1987**, *7*, 9.
[18] M. A. North, C. A. Del Grosso, J. J. Wilker, *ACS Appl. Mater. Interfaces* **2017**, *9*, 7866.
[19] L. Han, X. Lu, M. Wang, D. Gan, W. Deng, K. Wang, L. Fang, K. Liu, C. W. Chan, Y. Tang, L. T. Weng, H. Yuan, *Small* **2017**, *13*, 1601916.
[20] E. W. Danner, Y. Kan, M. U. Hammer, J. N. Israelachvili, J. H. Waite, *Biochemistry* **2012**, *51*, 6511.
[21] H. Zhao, N. B. Robertson, S. A. Jewhurst, J. H. Waite, *J. Biol. Chem.* **2006**, *281*, 11090.
[22] S. C. Warner, J. H. Waite, *Mar. Biol.* **1999**, *134*, 729.
[23] W. Wei, Y. Tan, N. R. Martinez Rodriguez, J. Yu, J. N. Israelachvili, J. H. Waite, *Acta Biomater.* **2014**, *10*, 1663.
[24] J. H. Waite, X. Qin, *Biochemistry* **2001**, *40*, 2887.
[25] N. D. Catron, H. Lee, P. B. Messersmith, *Biointerphases* **2006**, *1*, 134.
[26] J. H. Waite, *Ann. N. Y. Acad. Sci.* **1999**, *875*, 301.
[27] N. R. Martinez Rodriguez, S. Das, Y. Kaufman, W. Wei, J. N. Israelachvili, J. H. Waite, *Biomaterials* **2015**, *51*, 51.
[28] M. J. Sever, J. J. Wilker, *Dalton Trans.* **2006**, *16*, 813.
[29] B. P. Lee, C. Y. Chao, F. N. Nunalee, E. Motan, K. R. Shull, P. B. Messersmith, *Macromolecules* **2006**, *39*, 1740.
[30] M. P. Soriaga, A. T. Hubbard, *J. Am. Chem. Soc.* **1982**, *104*, 3937.
[31] H. Zhang, T. Zhao, B. Newland, W. Liu, W. Wang, W. Wang, *Prog. Polym. Sci.* **2018**, *78*, 47.
[32] J. H. Waite, M. L. Tanzer, *Science* **1981**, *212*, 1038.

© 2020 Wiley-VCH GmbH

[33] L. M. McDowell, L. A. Burzio, J. H. Waite, J. Schaefer, *J. Biol. Chem.* **1999**, *274*, 20293.
[34] B. P. Lee, J. L. Dalsin, P. B. Messersmith, *Biomacromolecules* **2002**, *3*, 1038.
[35] L. Han, X. Lu, K. Liu, K. Wang, L. Fang, L. T. Weng, H. Zhang, Y. Tang, F. Ren, C. Zhao, G. Sun, R. Liang, Z. Li, *ACS Nano* **2017**, *11*, 2561.
[36] J. Yu, Y. Kan, M. Rapp, E. Danner, W. Wei, S. Das, D. R. Miller, Y. Chen, J. H. Waite, J. N. Israelachvili, *Proc. Natl. Acad. Sci. USA* **2013**, *110*, 15680.
[37] W. Zhang, R. Wang, Z. Sun, X. Zhu, Q. Zhao, T. Zhang, A. Cholewinski, F. K. Yang, B. Zhao, R. Pinnaratip, P. K. Forooshani, B. P. Lee, *Chem. Soc. Rev.* **2020**, *49*, 433.
[38] D. Gan, T. Xu, W. Xing, X. Ge, L. Fang, K. Wang, F. Ren, X. Lu, *Adv. Funct. Mater.* **2019**, *29*, 1805964.
[39] Z. Jia, Y. Zeng, P. Tang, D. Gan, W. Xing, Y. Hou, K. Wang, C. Xie, X. Lu, *Chem. Mater.* **2019**, *31*, 5625.
[40] D. Gan, W. Xing, L. Jiang, J. Fang, C. Zhao, F. Ren, L. Fang, K. Wang, X. Lu, *Nat. Commun.* **2019**, *10*, 1487.
[41] S. Hong, K. Y. Kim, H. J. Wook, S. Y. Park, K. D. Lee, D. Y. Lee, H. Lee, *Nanomedicine* **2011**, *6*, 793.
[42] D. Kaneko, S. Wang, S. Taira, N. Hiraishi, S. Tateyama, K. Yasaki, A. Miyasato, A. Tsuge, T. Kaneko, *Int. Symp. Micro-NanoMechatronics and Human Science MHS2013*, IEEE, Nagoya, Japan **2013**.
[43] J. Jiang, Y. Huang, Y. Wang, H. Xu, M. Xing, W. Zhong, *Materials* **2017**, *10*, 964.
[44] Y. Yang, S. Ding, T. Araki, J. Jiu, T. Sugahara, J. Wang, J. Vanfleteren, T. Sekitani, K. Suganuma, *Nano Res.* **2016**, *9*, 401.
[45] K. Kojio, S. Nakashima, M. Furukawa, *Polymer* **2007**, *48*, 997.
[46] S. Liang, Y. Zhang, H. Wang, Z. Xu, J. Chen, R. Bao, B. Tan, Y. Cui, G. Fan, W. Wang, W. Wang, W. Liu, *Adv. Mater.* **2018**, *30*, 1704235.
[47] L. Han, L. Yan, K. Wang, L. Fang, H. Zhang, Y. Tang, Y. Ding, L.-T. Weng, J. Xu, J. Weng, Y. Liu, F. Ren, X. Lu, *NPG Asia Mater.* **2017**, *9*, e372.
[48] R. Wang, J. Li, W. Chen, T. Xu, S. Yun, Z. Xu, Z. Xu, T. Sato, B. Chi, H. Xu, *Adv. Funct. Mater.* **2017**, *27*, 1604894.
[49] W. Zhu, Y. J. Chuah, D. A. Wang, *Acta. Biomater.* **2018**, *74*, 1.
[50] G. P. Maier, M. V. Rapp, J. H. Waite, J. N. Israelachvili, A. Butler, *Science* **2015**, *349*, 628.
[51] X. Pei, H. Zhang, Y. Zhou, L. Zhou, J. Fu, *Mater. Horiz.* **2020**, *7*, 1872.
[52] X. Jing, H. Y. Mi, Y. J. Lin, E. Enriquez, X. F. Peng, L. S. Turng, *ACS Appl. Mater. Interfaces* **2018**, *10*, 20897.
[53] F. Yu, X. Cao, J. Du, G. Wang, X. Chen, *ACS Appl. Mater. Interfaces* **2015**, *7*, 24023.
[54] X. Liu, Q. Zhang, Z. Gao, R. Hou, G. Gao, *ACS Appl. Mater. Interfaces* **2017**, *9*, 17645.
[55] L. Han, L. Yan, M. Wang, K. Wang, L. Fang, J. Zhou, J. Fang, F. Ren, X. Lu, *Chem. Mater.* **2018**, *30*, 5561.
[56] H. Qiao, P. Qi, X. Zhang, L. Wang, Y. Tan, Z. Luan, Y. Xia, Y. Li, K. Sui, *Chem. Mater.* **2019**, *11*, 7755.
[57] D. Gan, W. Xing, L. Jiang, J. Fang, C. Zhao, F. Ren, L. Fang, K. Wang, X. Lu, *Nat. Commun.* **2019**, *10*, 1487.
[58] L. Han, M. Wang, L. O. Prieto-López, X. Deng, J. Cui, *Adv. Funct. Mater.* **2019**, *30*, 1907064.
[59] C. Cui, C. Fan, Y. Wu, M. Xiao, T. Wu, D. Zhang, X. Chen, B. Liu, Z. Xu, B. Qu, W. Liu, *Adv. Mater.* **2019**, *31*, 1905761.
[60] S. Ji, C. Wan, T. Wang, Q. Li, G. Chen, J. Wang, Z. Liu, H. Yang, X. Liu, X. Chen, *Adv. Mater.* **2020**, *32*, 2001496.
[61] H. Lee, N. F. Scherer, P. B. Messersmith, *Proc. Natl. Acad. Sci. USA* **2006**, *103*, 12999.
[62] J. H. Waite, *Comp. Biochem. Physiol.* **1990**, *97*, 19.
[63] W. Wei, L. Petrone, Y. Tan, H. Cai, J. N. Israelachvili, A. Miserez, J. H. Waite, *Adv. Funct. Mater.* **2016**, *26*, 3496.
[64] Y. Jin, D. Deng, Y. Cheng, L. Kong, F. Xiao, *Nanoscale* **2014**, *6*, 4812.
[65] T. Akter, W. S. Kim, *ACS Appl. Mater. Interfaces* **2012**, *4*, 1855.
[66] J. P. Gallivan, D. A. Dougherty, *J. Am. Chem. Soc.* **2000**, *122*, 870.
[67] J. Schnurrer, C. M. Lehr, *Int. J. Pharm.* **1996**, *141*, 251.
[68] J. H. Waite, *Int. J. Adhes. Adhes.* **1987**, *7*, 9.

© 2020 Wiley-VCH GmbH